HYDROGEN, FUEL CELL & ENERGY STORAGE

Thermodynamic and Thermoeconomic Analysis of the Use of Wind and Solar Energy to Supply the Energy Requirements of a Multigeneration System

Arash Garmabi | Sajad Rezazadeh* | Farzad Mohammadkhani

Department of Mechanical Engineering, Urmia University of Technology, Urmia, Iran
* Corresponding author, Email: sor.mems@gmail.com

Article Information

Article Type
Research Article

Article History
Received: *05 Nov 2025*
Revised: *22 Dec 2025*
Accepted: *14 Feb 2026*
Published Online: *08 Mar 2026*

Keywords

Multigeneration Energy System
Thermodynamic Analysis
Thermoeconomic Evaluation
Solar-Wind Hybrid Energy
Hydrogen and Freshwater Production

Abstract

The current paper provides a thermodynamic, and thermoeconomic analysis of a new multigenerational energy system consisting of the solar thermal energy source and the wind source. This consists of a Brayton cycle driven by a solar tower, a Steam Rankine Cycle (SRC) with feedwater heater and makeup condensate pump, an Organic Rankine Cycle with ejector refrigeration (ORC-ERC), a thermoelectric generator (TEG), a proton exchange membrane (PEM) electrolyzer and a reverse osmosis (RO) desalination plant so that electricity, hydrogen, freshwater, heating, cooling and domestic hot water are produced simultaneously. It has overall annual power output of 38.37 MW, thermal efficiency of 25.22% and exergy efficiency of 50.7%. The saltwater has a desalting rate of 0.008 kg/s and hydrogen at 19.37 kg/s. The greatest exergy losses can be found in the solar collector, compressors and the combustion chamber pointing out to the areas where improvements can be introduced. From Thermoeconomic point of view, gas turbine is deemed to be capital intensive and the solar collector and wind turbine are highly cost effective. Sensitivity studies show that raising the gas turbine inlet temperature and increment of the pressure ratio of the compressor will boost the performance considerably. All in all, the suggested pathway is not only a technically viable and financially beneficial model of clean, diversified energy production with affinities to locations that have plentiful resources of both solar and wind power.

Cite this article: Garmabi, A., Rezazadeh, S., Mohammadkhani, F. (2026). Thermodynamic and Thermoeconomic Analysis of the Use of Wind and Solar Energy to Supply the Energy Requirements of a Multigeneration System. DOI: 10.22104/hfe.2025.7766.1374

 Publisher: Iranian Research Organization for Science and Technology (IROST)
DOI: 10.22104/hfe.2025.7766.1374

1 Introduction

The global energy industry is facing some severe issues because the energy demand continues to increase and there is a growing concern about the sustainability of the environment. Conventional fossil energy, long used to fuel industry and households, has faced criticism over the years for its negative effects, including air pollution, greenhouse gas emissions, and the depletion of energy resources [1]. As a reaction, renewable sources have been emphasized with a noticeable turn toward wind and solar energy which have gradually become the key elements of the transformation process due to the high availability rates, inherent sustainability, and negligible environmental pollution rates. Solar and wind energy have a number of advantages that make them irreplaceable in developing sustainable energy systems. Both are renewable energy sources, unlike fossil fuels, which are consumable; they are naturally replenished and will not run out. Solar energy exploits the heat energy of the light of the sun whereas wind energy exploits the energy motion of moving air all of which are freely available in most parts of the world. Furthermore, it emits little greenhouse-gas emissions through the efficacious operations of the solar and the wind systems in moderating the climate change. More so, the systems are relatively less expensive to maintain once installed and utilized. Solar and Wind power are much less expensive in terms of long-term cost compared to the traditional power generating plants which rely on costly power generation costs as well as high recurrent costs. Since all these are sources of renewable energy, they improve the security of energy supply and reduce the extent of external dependency. Since the technological possibilities are increasing, the efficiency and storage capacity of the solar and wind sector continue to rise, making them even more appropriate to be used as the main sources of energy in grid transition to more clean and sustainable grids [2].

Even though the infrastructure of renewable energy has quite a range of benefits, the integration of these resources into the present-day networks of energy conveyance is combined with certain barriers. Wind and solar production have intermittent behavior (interrupted by wind stillness and night-time) and they are naturally intermittent in their output; this can create instability and lower system efficiency. Moreover, there is also a problem of having to accommodate renewable generation in the context of infrastructures already in place since most of them often fail to provide adequate capacity to absorb renewable generation in a way that will increase capacity utilization and on the other hand reduce expenses. An appropriate response to these limits would be amultigeneration system as a thought-provoking change. These systems are able to maximize the use of the available energy, reduce wastage, and to set a more efficient and sustainable paradigm of meeting the heterogeneous energy demand, since they can provide several energy services: electricity, thermal energy to heat or cool a given environment, and desalinated water by integrating various types of renewable energy [3]. The idea that wind power and solar power should be included in multigeneration architectures, allows a significant potential, but must be critically evaluated at thermodynamic/thermoeconomic levels. A thermodynamic appraisal explains the performance of a process of conversion, but the entire plant might not be economically and financially viable and effective, so a thermoeconomic analysis is required to understand that. Collectively, the approaches create a comprehensive structure of assessing renewable energy incorporation within multigeneration systems, thus helping the achievement of both environment-friendly and affordable goals.

Several researchers have done studies on the thermodynamic and thermoeconomic of multigeneration systems using renewable resource energy sources. Sharifishourabi et al. [4] explain a multigeneration platform that combines solar-thermal and geothermal technologies to produce electricity, cooling, heating, hot-water, and Hydrogen. The Brayton, solar Rankine and organic Rankine have energy efficiencies of 32.04%, 35.99% and 14.56%, respectively with their respective exergy efficiencies being 63.11%, 74.30% and 43.79%. This system reduces CO_2 emissions by 2.513 kg/kWh using this kind of configuration. Farghani et al. [5] designed an improved system of freshwater supply, space-heating, space-cooling and generating electricity based on renewable resources. Geothermal wells generating geothermal heat and flat plate collectors and photovoltaic panels harvesting solar energy were those used. After optimization, solar, geothermal, and the composite system attracted an improvement in the objective function of 14.38%, 54.61%, and 59.78%, respectively.

Azizi et al. [6] presented a multigeneration platform using solar energy that incorporates the generation of electricity, desalination and cooling of water, and the production of hydrogen. The numerical analysis showed at design operational conditions an electrical power of 7.871 MW, a potable water of 10.05 kg/s, a cooling capacity 8.788 MW thermal power, and a yield 0.2445 kg/h of hydrogen with an overall energy efficiency of 41.18%. Parametric studies were then carried out on large scale to determine the responses of systems to various input and operating parameters thus explaining performance sensitivity. Mahmoudan et al. [7] have discussed a multigeneration concept of heating,

cooling, electricity and desalinated water production. The desalination element was a reverse-osmosis unit and the cooling requirements were provided by a vapor-compression cycle. Using 3 energy system analysis and multi-objective optimization the authors showed that it was possible to obtain an exergy of 29.15%, an exergy unit cost of 1.5/GJ, and a desalinated water produced of 0.817 kg/s.

Li et al. [8] proposed the five-step framework to maximize the heat recovery of the binary flash geothermal power plant. The scheme was designed with the use of a desalination unit coupled with a dehumidification module and other auxiliary subsystems and an ejector refrigeration cycle. A multi-objective optimization analysis combining thermodynamic and economic constraints, revealed that the system achieves an exergy efficiency of 46.44%, a product cost of $3.98/GJ, and a water desalination rate of 0.286 kg/s. According to a recent analysis by Javadi et al. [9], a multigeneration scheme combines geothermal and solar energy through the two-by-two combination of a solar tower plant, an alkaline electrolyzer, and a single-stage absorption cycle to simultaneously achieve cooling, heating, electricity production, and hydrogen production. Based on energy, exergy, and exergoeconomic assessments, the researchers browse on the overall values of 19% and 19.29%, of energy and exergy efficiencies, respectively. An assessment and optimization of a solar-energy-collection system based on parabolic trough collector is provided in a research paper by Mahmoudan et al. [10]. The analysis shows that an exergy efficiency of 35.2% and a total cost of production of $37.8/GJ was possible with the system and at its optimum conditions. Such results support the fact that the system has a significant efficiency in the use of solar energy within multigeneration scenarios.

Mohammadi et al. [11] presented, evaluated, and optimized a new multigeneration platform operated on a dual renewable energy design (geothermal and solar). The system combines geothermal heat exchangers, solar tower receivers, Rankine cycle, ejector refrigeration sub-system, thermoelectric generator and a reverse osmosis (RO) unit. Optimization calculations indicate that 25.4% exergy efficiency and the total cost of products per GJ is of 34.1 $, 3.43 kg/s average and ranging 3.06-3.84 kg/s is the freshwater that is produced. Koc et al. [12] developed a new type of geothermal based multigeneration power plant that is meant to produce electricity, cooling, heating, pool heating, and hydrogen fuel simultaneously." Full thermodynamic and economical evaluation was done to optimize the layout and also to understand the interaction of the parameters that would change the plant performance. The investigations identified a total energy and exergy efficiency of 32.3% and 25.4% respectively. In addition, the cost of hydrogen production may be reduced to USD 1.06/kg. Khan and co-workers [13] followed exergoeconomic analysis of a hybrid nanofluid-based multigeneration scheme which combined fitting of electricity, hydrogen, cooling and desalinated water. The configuration – supply driven by a solar dish collector – was designed with a series of a Brayton cycle, absorption cycle, electrolyzer and desalination unit. Phase-change material warming /cooling store provided night-time energy. The LCOE of electricity production of the unit with energy storage was US$0.14 kWh^{-1} and without storage US$0.35 kWh^{-1}. The estimated energy efficiencies were 31.4% for electrical production and 30% for total exergy, respectively.

Ding et al. [14] explore on Kalina cycle, organic Rankine cycle, refrigeration, electrolysis, and thermoelectric generation-based integrated solar geothermal energy system. The geothermal wells, parabolic trough collectors and biomass combustion provide thermal input. The setting provides a maximum power of 80.1 kW of electricity and 1930 g/h of hydrogen, under the best operating conditions. Sen et al. [15] offer a rather thorough modelling and analysis of a multi-generation energy system combining geothermal and solar energy resources to electrify households in their paper. The suggested system is a hybrid geothermal electricity generator, which is combined with a parabolic solar concentrator, an electrolyzer, and a hydrogen fuel cell to store and use the hydrogen. This arrangement, at steady-state, has an electricity generation capacity of 2900 kW and hydrogen yield of 0.0185 kg/s or 5.9% energy efficiency and 18.99% exergy efficiency.

Guler et al. [16] compared and evaluated a multigeneration system based on the combined use of geothermal and solar energy. Three conceptual schemes were analyzed: Model 1 had a single-stage parabolic collector, Model 2 a twin-stage parabolic collector and Model 3 a flat plate collector and indirect steam generation. The efficiencies of exergy in each of the systems were 32.1% and 32.4% and 30.6% respectively whereas the costs of hydrogen generation ranged narrowly within 1.55 to 1.58 dollars per kilogram. Sezar and Koc [17] considered a new multigeneration system using solar and wind renewable energy sources, connected in a configuration that allows the simultaneous production of several outputs: hydrogen, oxygen, desalinated water, cooling, and electricity. Through thermodynamic analysis of the system, there were overall energy and exergy efficiencies of 73.3 and 30.6 respectively. A detailed analysis of a solar-wind multigeneration system was also carried out by Ozlu and Dincer [18] using energy, exergy, exergoeconomic and environmental parameters. They were studying

the effects of varying input conditions upon the general performance of the system. The hybrid installation had the best energy and exergy efficiency of 43% and 65%, respectively. At 48 kW, the turbine reached its maximum output; the refrigeration load was 28 kW, and the space heater load was 298.5 kW. Such setup avoided 1614 tons of CO_2 per year.

Nasrabadi and Korpeh [19] provided a thermo-economic evaluation of a multigeneration plant to combine a solar photovoltaic and a wind turbine renewable energy source. The installation is such that it produces electricity, desalinated water and hydrogen all at once. The plant includes solar collectors, a solar thermal steam Rankine subsystem, an organic Rankine subsystem, a desalination system, and a hydrogen system for production and compression. A thermodynamic study gave the exergy efficiency of 33.3% and the production of hydrogen 7.92 kg/h, the production of freshwater 1.6398 kg /s and the total cost rate was found to be 61.28 $/h. A multigenerational system, which combined solar and geothermal energy with the purpose of creating electricity, production of hydrogen, cooling, and space-heat was evaluated by the research by Ghrairi et al. [20]. The total energy efficiency of the system was 41.58% and the exergy efficiency was 25.61%. It delivered 493.1 kg/day of hydrogen and its performance was later optimized, making it ready to be deployed effectively to renewable energy source. Abdollahi et al. [21] have created a multigeneration platform whereby geothermal resources are utilized in the generation of power, the production of fresh water, the synthesis of hydrogen and provision of process heat. The designed conceptual scheme incorporates an ammonia water absorption refrigeration hydrogen precooling circuit and a follow up hydrogen liquefaction one. A cost of $2.71/kg in hydrogen production and 8.51 kWh/kg of specific energy consumption are the result of their thorough energy, exergy, and economic analysis.

According to a systematic review of published studies, multigeneration systems represent a relatively novel area of research that has not received the same level of attention as trigeneration systems. Solar irradiance plays an important role as the leading energy source in most reported settings. The recent investments have been made in the combination of various goods carriers, which can be regarded as a relevant improvement, but wind power has hardly ever been mentioned as a secondary energy alternative used in multigeneration activities, therefore, revealing a massive knowledge gap. The given research proposes a novel combination of solar and wind energy to use together as the primary sources as the means of multigeneration. The gas turbine cycles, Rankine steam cycles, organic Rankine cycles, and desalination plants are driven by the solar irradiance and electricity generated by wind energy is supplied to a proton exchange membrane (PEM) electrolyzer. The integration of solar and wind in a multigeneration platform, especially when combined with the new PEM electrolyzer technology, has not been extensively studied in the literature and therefore represents a novel contribution.

The remainder of this paper reads as follows. Section 2 gives the design characteristic of the proposed solar-wind multigeneration system. Section 3 gives details of the simulation technique and thermodynamic hypothesis. In section 4, we perform thermo-economic analysis whose preparation is based on the thermodynamic results. The practicality of the system as well as some cross comparisons strengths and possible applications are discussed in the conclusion in section 6. This work presents the following contributions: (i) the creation of a hybrid solar-wind multigeneration scenario integrating electricity, hydrogen, freshwater, heating, and cooling; (ii) a combination of thermodynamic and thermo-economic analysis, supplemented with a sensitivity study; (iii) a comparative view of the proposed system to that of a common trigeneration and polygeneration scheme.

2 System Description

Figure 1 is the schematic diagram of the proposed multigenerational system. The system involves two renewable energy sources (solar thermal and wind power) to produce electricity, domestic hot water, fresh water, hydrogen and thermal energy simultaneously. The heart of the system is solar radiation which is focused on a solar-thermal tower, thus serving as the actual heat source of a Brayton-cycle gas turbine. The concentrated solar radiation heats the compressed air, which is then further heated in an auxiliary combustor to create a stream of high-temperature gases that expand in the turbine to produce useful electrical power. The exhaust gases of the turbine are not exhausted; instead, they are deliberately recaptured to serve two other heat cycles, one being steam-Rankine-cycle (SRC) and the other being organic-Rankine-cycle combined with ejector refrigeration cycle (ORC-ERC). The SRC uses the heat of exhausts to produce extra electricity through steam expansion, whereas the ORC-ERC works with organic working substances and consists of a pump, a preheater, main and side evaporators, a turbine, an ejector, a condenser and an expansion valve. The ejector enhances the energy-recovery ratio because of entraining low-pressure vapour and being highly mixed, which boosts thermodynamic performance and the ability to partially cool within the cycle. Furthermore, this system involves a reverse osmosis (RO) desalina-

tion unit which is electrically powered, by the gas turbine, the steam turbine recovered in the SRC and an auxiliary thermoelectric generator (TEG). In addition, a proton-exchange-membrane (PEM) electrolyzer is installed to produce hydrogen which can be supplied with electrical power by the wind turbine and excessive electricity generated inside the ORC-ERC subsystem.

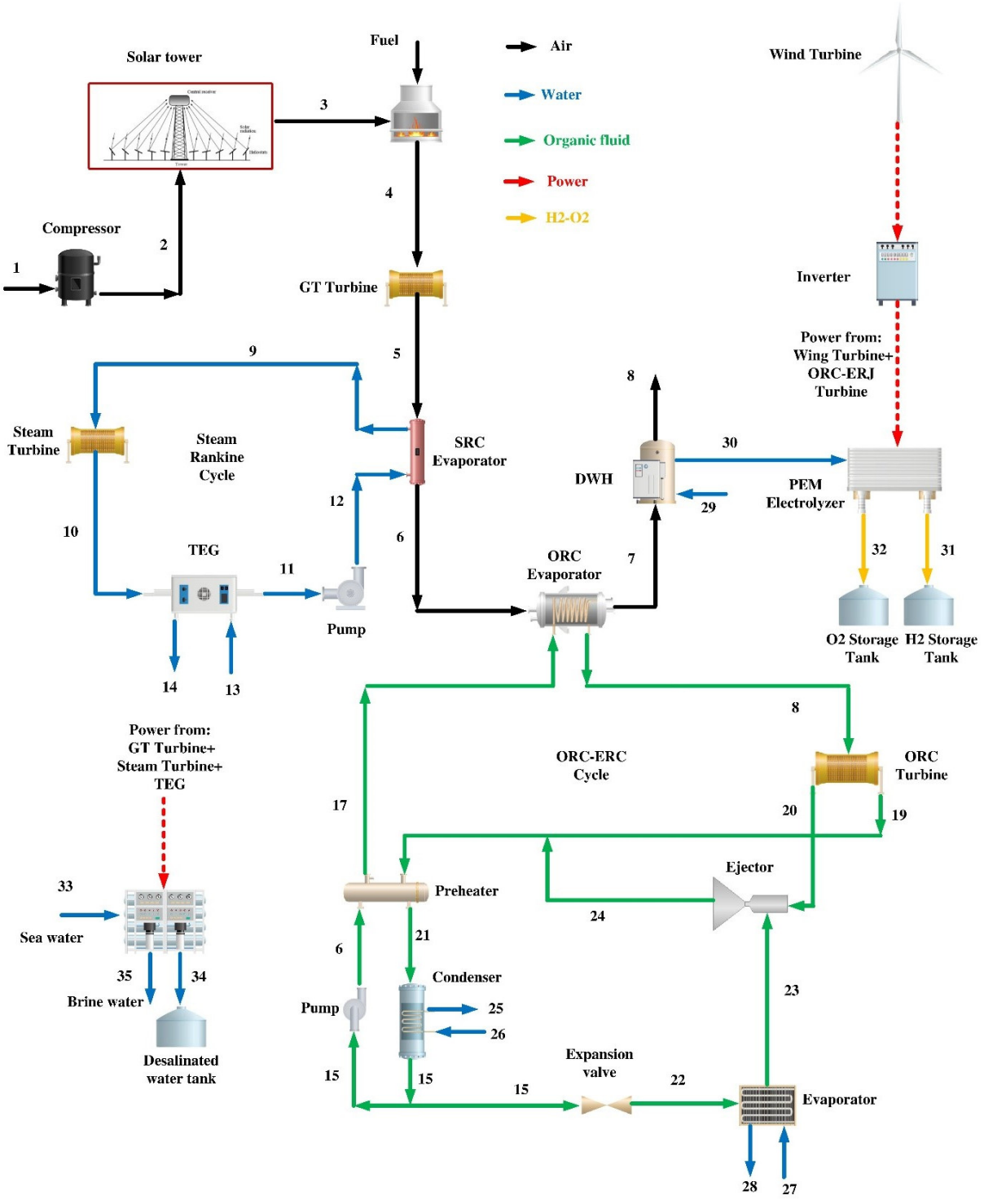

Fig. 1. The schematic diagram of the solar-Wind energy based multigeneration system.

3 System Modeling

3.1 Assumptions

This paper is an account of thermodynamic modeling and analysis of a multigeneration cycle, in which a number of simplifying assumptions can be made, to allow easier interpretation of the outcomes. The assumptions are the following:

1. System components experience negligible pressure drops and heat losses in the pipes.
2. All components are perfectly insulated and considered adiabatic.
3. The steady-state operation of the whole system and also, the subsystems.
4. Minor alterations of Kinetic and potential energy.
5. All pumps, turbines had isentropic efficiencies.
6. There are no other chemical reactions except that in combustion chamber.
7. No wastage of heat in the combustion chamber.
8. Continuous and constant sunshine.
9. Abrupt changes in electricity demand due to wind turbine fluctuations are not considered.

We have adopted these simplifications because they are common in the literature on multigeneration systems and because it simplifies the analysis without speaking to the relative merits of the various approaches. Under such ideal assumptions of insulation, negligible pressure drops and steady operation, the sizing calculations of the main performance of the overall system can be sized without being lost in minor secondary losses or short term variations. By considering solar radiation and wind speed as constant, it is merely a means of thinking about design conditions in the most favorable way, to gain a feel of how the system will perform under perfect conditions. These assumptions are, of course, very idealized, and can make results a bit overly healthy as there will be real world variance that will not be prevalent in the results. The results here must therefore be considered purely a reference point, and future simulations that represent the real situation with more dynamic conditions will be necessary to provide a near representation of the possibility in a real system.

With these assumptions a mathematical model of the cycle was developed and solved numerically by software known as Engineering Equation Solver (EES) [22] and has been used extensively by researchers to easily and conveniently model and run high fidelity simulations of energy systems.

There are a number of requirements that must be met before there is numerical modeling of a multigenerational system as the current study demands. All of these requirements and, the original thermodynamic input parameters are presented in Table 1.

Table 1. Assumed numerical values for solar and wind energy system modeling [23–26]

Parameters	Unit	Value
Ambient temperature (T_0)	K	298
Ambient pressure (P_0)	kPa	101
Solar Tower		
Heliostat area (A_h)	m^2	100
Solar radiation (G)	W/m^2	500
Sun temperature	K	5778
Gas Turbine Cycle		
Air mass flow rate ($\dot{m}_1$)	Kg/s	30
Compressor pressure ratio (r_p)	-	12
Turbine inlet temperature (T_4)	K	1400
Compressor isentropic efficiency ($\eta_{is,comp}$)	%	86
Turbine isentropic efficiency ($\eta_{is,GT}$)	%	90
Steam Rankine Cycle		
Turbine inlet temperature (T_9)	K	723
Turbine isentropic efficiency ($\eta_{is,SRCtur}$)	%	80
Pump isentropic efficiency ($\eta_{is,SRCP}$)	%	90
ORC-ERC		
Working fluid	-	Isobutane
Pump inlet temperature (T_{15})	K	298
Turbine inlet temperature (T_{18})	K	423
Evaporator inlet temperature (T_{25})	K	273
Turbine isentropic efficiency ($\eta_{is,ORCtur}$)	%	80
Pump isentropic efficiency ($\eta_{is,ORCP}$)	%	80
Wind Turbine		
Dimeter of blade	m	34
Air density	kg/m^3	1.225
Efficiency (η_{wt})	%	90
Wind speed	m/s	5.5
Coefficient of power	-	0.6
TEG		
Figure of merit (ZT)	-	1
PEM electrolyzer		
Current density	A/m^2	5100
Membrane water content at the anode (λ_a)	-	14
Membrane water content at the cathode (λ_c)	-	10
Anode pre-exponential factor ($J_{ref,a}$)	kA/m^2	2000

Table 1. (*Continued*)

Parameters	Unit	Value
Cathode pre-exponential factor ($J_{\mathrm{ref},c}$)	kA/m^2	4600
Membrane thickness (D)	μm	50
Anode activation energy ($E_{\mathrm{act},a}$)	kJ/mol	76
Cathode activation energy ($E_{\mathrm{act},c}$)	kJ/mol	18
Reverse osmosis desalination unit		
Recovery ratio	-	0.3
Highest applied pressure	MPa	6.89
Membrane area	m^2	35.
Highest permeate-flux	L/m^{2}s	47
Permeability of pure water	kg/msPa	2.5×10^{-9}
Efficiency (η_{RO})	%	80

3.2 Thermodynamic analysis

Under steady-state conditions, the mass balance equation exists in form shown by Equation (1) as [27]:

$$\sum \dot{m}_{\mathrm{in}} - \sum \dot{m}_{\mathrm{out}} = \frac{dm_{\mathrm{cv}}}{dt}\,. \tag{1}$$

The energy balance equation in a general form can be defined as Equation (2) [27]:

$$\dot{Q} - \dot{W} + \sum_{\mathrm{in}} \dot{m}_{\mathrm{in}}\left(h_{\mathrm{in}} + \frac{V_{\mathrm{in}}^2}{2} + gZ_{\mathrm{in}}\right) - \sum_{\mathrm{out}} \dot{m}_{\mathrm{out}}\left(h_{\mathrm{out}} + \frac{V_{\mathrm{out}}^2}{2} + gZ_{\mathrm{out}}\right) = \frac{dE_{\mathrm{cv}}}{dt}\,. \tag{2}$$

In this equation, $\dot{W}$, $\dot{Q}$, E and t represent the work rate, heat transfer rate, energy and time. According to the second law of thermodynamics, the exergy balance can be expressed as:

$$\dot{\mathrm{E}}\mathrm{x}_Q + \sum_{\mathrm{in}} \dot{m}_{\mathrm{in}}\mathrm{ex}_{\mathrm{in}} = \sum_{\mathrm{out}} \dot{m}_{\mathrm{out}}\mathrm{ex}_{\mathrm{out}} + \dot{\mathrm{E}}\mathrm{x}_W + \dot{\mathrm{E}}\mathrm{x}_D\,. \tag{3}$$

In this equation, $\dot{\mathrm{E}}\mathrm{x}_D$ is the exergy destruction rate, $\dot{\mathrm{E}}\mathrm{x}_Q$ is the heat exergy rate, $\dot{\mathrm{E}}\mathrm{x}_W$ is the work exergy rate, and ex is the specific exergy.

The other components of the above relationship are calculated using the following relationships:

$$\dot{\mathrm{E}}\mathrm{x}_Q = \left(1 - \frac{T_0}{T_i}\right)\dot{Q}_i\,, \tag{4}$$

$$\dot{\mathrm{E}}\mathrm{x}_W = \dot{W}\,, \tag{5}$$

$$\mathrm{ex} = \mathrm{ex}_{\mathrm{ph}} + \mathrm{ex}_{\mathrm{ch}}\,. \tag{6}$$

The Table 2 summarizes the mass and energy rates and gives the associated exergy destruction rate equations.

3.2.1 Solar tower heliostat

The total heat received by the compressed air can be defined as [28]:

$$\dot{Q}_{\mathrm{rec}} = A_h \times N_h \times \mathrm{DNI} \times \eta_{\mathrm{rec}} \tag{7}$$

where $\dot{Q}_{\mathrm{rec}}$ is the total heat reaching the compressed air through the solar collector, A_h is the heliostat area, N_h is the number of heliostats, η_{rec} is the efficiency of the solar collector, and DNI represents the solar radiation rate.

The exergy rate of heat transfer in the solar receiver can also be calculated from the following equation:

$$\dot{\mathrm{E}}\mathrm{x}_{\mathrm{solar}} = \dot{Q}_{\mathrm{rec}}\left(1 + \frac{1}{3}\left(\frac{T_0}{T_s}\right)^4 - \frac{4}{3}\left(\frac{T_0}{T_s}\right)\right) \tag{8}$$

3.2.2 Combustion chamber

Combustion chambers are a key element in most thermal power plants where combustion occurs and the enthalpy of the flow increases. In most of the studies, complete combustion is assumed and the fuel-air ratio is calculated. In this study, we consider actual combustion in real power plants. Therefore, CO and NO can be calculated using equilibrium constants. The reaction in the combustion chamber can be represented by the following equation [29]:

$$y_{\mathrm{CH_4}}\mathrm{CH_4} + \left(0.2059\,y_{\mathrm{O_2}} + 0.7748\,y_{\mathrm{N_2}} + 0.019\,y_{\mathrm{H_2O}} + 0.0003\,y_{\mathrm{CO_2}}\right) \rightarrow y_{\mathrm{CO_2}}\mathrm{CO_2} + y_{\mathrm{N_2}}\mathrm{N_2} + y_{\mathrm{O_2}}\mathrm{O_2} + y_{\mathrm{H_2O}}\mathrm{H_2O} + y_{\mathrm{NO}}\mathrm{NO} + y_{\mathrm{CO}}\mathrm{CO} \tag{9}$$

The reactions and their equilibrium constants are written as the following equations:

$$2\,\mathrm{CO_2} \longleftrightarrow 2\,\mathrm{CO} + \mathrm{O_2}$$

$$K_{\mathrm{eq}}^{\mathrm{CO}} = \frac{-816518253.317 + 244902.10\,T}{1 + 23494.22\,T + 0.312\,T^2}\,, \tag{10}$$

$$\mathrm{N_2} + \mathrm{O_2} \longleftrightarrow 2\,\mathrm{NO}$$

$$K_{\mathrm{eq}}^{\mathrm{NO}} = \frac{-6635.17 + 0.89\,T}{1 + 0.6\,T + 6.5 \times 10^{-6}\,T^2}\,. \tag{11}$$

3.2.3 Wind turbine

The average power produced by a wind turbine is calculated as follows [30]:

$$P_{\mathrm{wt}} = \frac{1}{2}\eta_{\mathrm{wt}} A_{\mathrm{wt}} C_p \rho_{\mathrm{air}} V^3 \tag{12}$$

Here η_{wt} represents the efficiency of the wind turbine, A_{wt} is the area of the wind turbine (m^2), C_P is the power constant of the wind turbine, ρ is the air density (kg/m^3), and V is the average wind speed (m^2/s).

Table 2. Expression of the first law of thermodynamics and exergy destruction rate for system components

Components	Energy balance equation	Exergy destruction rate
GT Compressor	$\dot{m}_1 h_1 + \dot{W} = \dot{m}_2 h_2$	$\dot{\mathrm{E}}\mathrm{x}_{d,\mathrm{comp}} = \dot{m}_1 \mathrm{ex}_1 - \dot{m}_2 \mathrm{ex}_2 + \dot{W}_{\mathrm{comp}}$
Solar Tower	$\dot{m}_2 h_2 + \dot{Q}_{\mathrm{rec}} = \dot{m}_3 h_3$	$\dot{\mathrm{E}}\mathrm{x}_{d,\mathrm{st}} = \dot{m}_2 \mathrm{ex}_2 - \dot{m}_3 \mathrm{ex}_3 + \dot{Q}_{\mathrm{rec}} \left[1 + \frac{1}{3}\left(\frac{T_0}{T_s}\right)^4 - \frac{4}{3}\left(\frac{T_0}{T_s}\right)\right]$
Combustion Chamber	$\dot{m}_3 h_3 + \dot{m}_{\mathrm{fuel}} h_{\mathrm{fuel}} = \dot{m}_4 h_4 + \dot{Q}^{\mathrm{cc}}_{\mathrm{loss}}$	$\dot{\mathrm{E}}\mathrm{x}_{d,\mathrm{cc}} = \dot{m}_3 \mathrm{ex}_3 + \dot{m}_{\mathrm{fuel}} \mathrm{ex}_{\mathrm{fuel}} - \dot{m}_4 \mathrm{ex}_4$
GT Turbine	$\dot{m}_4 h_4 = \dot{m}_5 h_5 + \dot{W}_{GT}$	$\dot{\mathrm{E}}\mathrm{x}_{d,\mathrm{GT}} = \dot{m}_4 \mathrm{ex}_4 - \dot{m}_5 \mathrm{ex}_5 - \dot{W}_{GT}$
SRC Evaporator	$\dot{m}_5 h_5 + \dot{m}_{12} h_{12} = \dot{m}_6 h_6 + \dot{m}_9 h_9$	$\dot{\mathrm{E}}\mathrm{x}_{d,\mathrm{SRCeva}} = \dot{m}_5 \mathrm{ex}_5 - \dot{m}_6 \mathrm{ex}_6 + \dot{m}_{12} \mathrm{ex}_{12} - \dot{m}_9 \mathrm{ex}_9$
SRC Turbine	$\dot{m}_{10} h_{10} + \dot{W}_{\mathrm{SRCtur}} = \dot{m}_9 h_9$	$\dot{\mathrm{E}}\mathrm{x}_{d,\mathrm{SRCtur}} = \dot{m}_9 \mathrm{ex}_9 - \dot{m}_{10} \mathrm{ex}_{10} + \dot{W}_{\mathrm{SRCtur}}$
TEG	$\dot{m}_{10} h_{10} + \dot{m}_{13} h_{13} = \dot{m}_{11} h_{11} + \dot{m}_{14} h_{14} - \dot{W}_{\mathrm{TEG}}$	$\dot{\mathrm{E}}\mathrm{x}_{d,\mathrm{TEG}} = \dot{m}_{10} \mathrm{ex}_{10} - \dot{m}_{11} \mathrm{ex}_{11} + \dot{m}_{13} \mathrm{ex}_{13} - \dot{m}_{14} \mathrm{ex}_{14} - \dot{W}_{\mathrm{TEG}}$
SRC Pump	$\dot{m}_{11} h_{11} + \dot{W}_{\mathrm{SRCP}} = \dot{m}_{12} h_{12}$	$\dot{\mathrm{E}}\mathrm{x}_{d,\mathrm{SRCP}} = \dot{m}_{11} \mathrm{ex}_{11} - \dot{m}_{12} \mathrm{ex}_{12} + \dot{W}_{SRCP}$
ORC Evaporator	$\dot{m}_6 h_6 + \dot{m}_{17} h_{17} = \dot{m}_7 h_7 + \dot{m}_{18} h_{18}$	$\dot{\mathrm{E}}\mathrm{x}_{d,\mathrm{ORCeva}} = \dot{m}_6 \mathrm{ex}_6 - \dot{m}_7 \mathrm{ex}_7 + \dot{m}_{17} \mathrm{ex}_{17} - \dot{m}_{18} \mathrm{ex}_{18}$
ORC Turbine	$\dot{m}_{18} h_{18} = \dot{m}_{19} h_{19} + \dot{m}_{20} h_{20} + \dot{W}_{\mathrm{ORCtur}}$	$\dot{\mathrm{E}}\mathrm{x}_{d,\mathrm{ORCtur}} = \dot{m}_{18} \mathrm{ex}_{18} - \dot{m}_{19} \mathrm{ex}_{19} - \dot{m}_{20} \mathrm{ex}_{20} + \dot{W}_{\mathrm{ORCtur}}$
Preheater	$\dot{m}_{16} h_{16} + \dot{m}_{21} h_{21} = \dot{m}_{17} h_{17} + \dot{m}_{22} h_{22}$	$\dot{\mathrm{E}}\mathrm{x}_{d,\mathrm{ORCpreh}} = \dot{m}_{16} \mathrm{ex}_{16} - \dot{m}_{17} \mathrm{ex}_{17} + \dot{m}_{21} \mathrm{ex}_{21} - \dot{m}_{22} \mathrm{ex}_{22}$
Pump	$\dot{m}_{15} h_{15} + \dot{W}_{\mathrm{ORCP}} = \dot{m}_{16} h_{16}$	$\dot{\mathrm{E}}\mathrm{x}_{d,\mathrm{ORCP}} = \dot{m}_{15} \mathrm{ex}_{15} - \dot{m}_{16} \mathrm{ex}_{16} + \dot{W}_{\mathrm{ORCP}}$
Condenser	$\dot{m}_{22} h_{22} + \dot{m}_{28} h_{28} = \dot{m}_{23} h_{23} + \dot{m}_{29} h_{29}$	$\dot{\mathrm{E}}\mathrm{x}_{d,\mathrm{ORCcon}} = \dot{m}_{22} \mathrm{ex}_{22} - \dot{m}_{23} \mathrm{ex}_{23} + \dot{m}_{28} \mathrm{ex}_{28} - \dot{m}_{29} \mathrm{ex}_{29}$
Expansion Valve	$\dot{m}_{24} h_{24} = \dot{m}_{25} h_{25}$	$\dot{\mathrm{E}}\mathrm{x}_{d,\mathrm{EXV}} = \dot{m}_{24} \mathrm{ex}_{24} - \dot{m}_{25} \mathrm{ex}_{25}$
Evaporator	$\dot{m}_{25} h_{25} + \dot{m}_{30} h_{30} = \dot{m}_{26} h_{26} + \dot{m}_{31} h_{31}$	$\dot{\mathrm{E}}\mathrm{x}_{d,\mathrm{eva}} = \dot{m}_{25} \mathrm{ex}_{25} - \dot{m}_{26} \mathrm{ex}_{26} + \dot{m}_{30} \mathrm{ex}_{30} - \dot{m}_{31} \mathrm{ex}_{31}$
Ejector	$\mu_{\mathrm{EJE}} = \frac{\dot{m}_{26}}{\dot{m}_{20}}$	$\dot{\mathrm{E}}\mathrm{x}_{d,\mathrm{EJE}} = \dot{m}_{20} \mathrm{ex}_{20} + \dot{m}_{26} \mathrm{ex}_{26} - \dot{m}_{27} \mathrm{ex}_{27}$
DWH	$\dot{m}_7 h_7 + \dot{m}_{32} h_{32} = \dot{m}_8 h_8 + \dot{m}_{33} h_{33}$	$\dot{\mathrm{E}}\mathrm{x}_{d,\mathrm{DWH}} = \dot{m}_7 \mathrm{ex}_7 - \dot{m}_8 \mathrm{ex}_8 + \dot{m}_{32} \mathrm{ex}_{32} - \dot{m}_{33} \mathrm{ex}_{33}$
Wind Turbine	$P_{\mathrm{wt}} = \frac{1}{2}\eta_{\mathrm{wt}} A_{\mathrm{wt}} C_p \rho_{\mathrm{air}} V^3$	$\dot{\mathrm{E}}\mathrm{x}_{d,WT} = \left(\frac{1}{C_{P,WT}} - 1\right) \times \dot{W}_{\mathrm{wt}}$
PEM Electrolyzer	$\dot{W}_{\mathrm{PEM}} = \dot{m}_{33} h_{33} - \dot{m}_{34} h_{34} - \dot{m}_{35} h_{35}$	$\dot{\mathrm{E}}\mathrm{x}_{d,\mathrm{PEM}} = \dot{m}_{33} \mathrm{ex}_{33} - \dot{m}_{34} \mathrm{ex}_{34} - \dot{m}_{35} \mathrm{ex}_{35} + \dot{W}_{\mathrm{PEM}}$
RO desalination unit	$\dot{W}_{\mathrm{RO}} = \dot{m}_{36} h_{36} - \dot{m}_{37} h_{37} - \dot{m}_{38} h_{38}$	$\dot{\mathrm{E}}\mathrm{x}_{d,\mathrm{RO}} = \dot{m}_{36} \mathrm{ex}_{36} - \dot{m}_{37} \mathrm{ex}_{37} - \dot{m}_{38} \mathrm{ex}_{38}$

The exergy rate for the turbine can be written as:

$$\dot{\mathrm{E}}\mathrm{x}_{\mathrm{wt}} = \frac{1}{2} A_{\mathrm{wt}} \rho_{\mathrm{air}} V^3 \tag{13}$$

and the exergy efficiency is expressed as follows:

$$\eta_{\mathrm{ex}} = \frac{\dot{W}_{\mathrm{wt}}}{\dot{\mathrm{E}}\mathrm{x}_{\mathrm{wt}}} \tag{14}$$

3.3 Thermoeconomic analysis

Thermoeconomics is a branch of engineering that arises from the integration of thermodynamics and economics. In the context of economic analysis, the overall cost balance for the entire system is expressed as follows [31]:

$$\dot{C}_{p,\mathrm{tot}} = \dot{C}_{F,\mathrm{tot}} + \dot{Z}^{\mathrm{CI}}_{\mathrm{tot}} + \dot{Z}^{\mathrm{O\&M}}_{\mathrm{tot}} \tag{15}$$

The cost rate related to fuel and product can be related to the cost rate related to the input and output flow of materials from the system, heat transfer, and power, and is expressed as follows:

$$\dot{C}_i = c_i = \dot{\mathrm{E}}\mathrm{x}_i\,, \tag{16}$$

$$\dot{C}_e = c_e \dot{\mathrm{E}}\mathrm{x}_e\,, \tag{17}$$

$$\dot{C}_W = c_W \dot{W}\,, \tag{18}$$

$$\dot{C}_q = c_q \dot{\mathrm{E}}\mathrm{x}_q\,. \tag{19}$$

In the above equations, c_i, c_e, c_w, and c_q represent the average unit exergy cost of the input flow, output flow, power, and heat transfer, respectively, in dollars per kilowatt.

The cost function for each component is used to determine the cost associated with each system component and the total cost rate. The total cost rate is calculated by applying economic factors such as the capital recovery factor and interest rate, allowing for a more accurate assessment of the system cost. The cost rate for each component is as follows:

$$\dot{Z}_k = \frac{Z_k \times \varphi \times \mathrm{CRF}}{\tau} \tag{20}$$

where Z_k represents the cost of each component, φ represents the maintenance factor and its value is 1.06. τ is the number of hours the system operates [32]. The capital recovery factor is defined as follows:

$$\mathrm{CRF} = \frac{i_r(1+i_r)^n}{(1+i_r)^n - 1} \tag{21}$$

In this equation, i and n represent the interest rate and the system lifetime, respectively, and are equal to 0.1 and 20.

The exergoeconomic factor is defined as follows:

$$f = \frac{\dot{Z}}{\dot{Z} + \dot{C}_D} \tag{22}$$

The functional relationships of the cost of purchased equipment in terms of the design parameters of each component are presented in Table 3.

Table 3. Investment costs of the proposed system components

Component	Purchase cost function
GT Compressor	$Z_{\mathrm{comp}} = 71.1 \times \dot{m}_1 \times \left(\frac{1}{0.9-\eta_{\mathrm{is,comp}}}\right) \times \left(\frac{P_2}{P_1}\right) \ln\left(\frac{P_2}{P_1}\right)$
Solar Tower	$Z_{\mathrm{st}} = 150 A_h N_h$
Combustion Chamber	$Z_{CC} = \left(\frac{48}{0.995-\frac{P_4}{P_3}}\right) \dot{m}_3 \left[1+\exp\left(0.018T_4 - 26.4\right)\right]$
GT Turbine	$Z_{\mathrm{GT}} = 479.34 \times \dot{m}_4 \times \left(\frac{1}{0.92-\eta_{\mathrm{is,GT}}}\right) \times \ln\left(\frac{P_4}{P_5}\right) \left[1+\exp\left(0.036T_4 - 54.4\right)\right]$
Evaporator	$Z_{\mathrm{eva}} = 17500 \times \left(\frac{A_{\mathrm{eva}}}{100}\right)^{0.6}$
Turbine	$Z_{\mathrm{tur}} = 4750 \times \left(\dot{W}_{\mathrm{tur}}\right)^{0.75}$
TEG	$Z_{\mathrm{TEG}} = 1500 \times \dot{W}_{\mathrm{TEG}}$
Pump	$Z_P = 200 \times \left(\dot{W}_P\right)^{0.65}$
Preheater	$Z_{\mathrm{preh}} = 12000 \times \left(\frac{A_{\mathrm{preh}}}{100}\right)^{0.6}$
Condenser	$Z_{\mathrm{con}} = 8000 \times \left(\frac{A_{\mathrm{con}}}{100}\right)^{0.6}$
Expansion Valve	$Z_{\mathrm{EXV}} = 114.5 \times \dot{m}_{24}$
Ejector	$Z_{\mathrm{EJE}} = 750 \times \dot{m}_{20} \times \left(\frac{T_{26}}{P_{26}}\right)^{0.05} \times (P_{21})^{-0.75}$
DWH	$Z_{\mathrm{DWH}} = 0.3 \times \dot{m}_7$
Wind Turbine	$Z_{\mathrm{wt}} = 5000 \times \dot{W}_{\mathrm{wt}}$
PEM Electrolyzer	$Z_{\mathrm{PEM}} = 1000 \times \dot{W}_{\mathrm{PEM}}$
RO desalination unit	$Z_{\mathrm{RO}} = c_k \times n_v \times n_e + c_{\mathrm{pv}} \times n_v + 996 \times (\dot{m}_{37})^{0.8}$

Table 4 shows the auxiliary equations of each system component and the cost rate equilibrium.

4 Validation

To verify the accuracy of the proposed multigeneration system modeling, it is important to compare the results of the modeled subsystems with other studies that have used the same input values for validation. For this purpose, the results of the solar tower subsystem have been compared with previous studies, and the findings are presented in Table 5. In addition, the performance of the gas Brayton cycle and the ejector refrigeration subsystem has been benchmarked against published data,

with the comparative results shown in Tables 6 and 7. As can be observed from these tables, the values obtained in this study are in very close agreement with reference values reported in the literature, confirming the accuracy of the proposed modeling approach.

Table 4. Cost rate equilibrium equations and auxiliary equations of the components of the proposed system.

Components	Cost rate balance	Auxiliary equation
GT Compressor	$\dot{C}_1 + c_{\text{el,comp}}\dot{W}_{\text{comp}} + \dot{Z}_{\text{comp}} = \dot{C}_2$	$c_1 = 0$
Solar Tower	$\dot{C}_2 + c_{\text{sun}}\dot{\text{Ex}}_{f,\text{ST}} + \dot{Z}_{\text{ST}} = \dot{C}_3$	$c_{\text{sun}} = 0$
Combustion Chamber	$\dot{C}_3 + c_{\text{fuel}}\dot{\text{Ex}}_{\text{fuel}} + \dot{Z}_{\text{cc}} = \dot{C}_4$	$c_{\text{fuel}} = 12$
GT Turbine	$\dot{C}_4 + \dot{Z}_{\text{GT}} = \dot{C}_5 + c_{\text{el,GT}}\dot{W}_{\text{GT}}$	$c_4 = c_5$
SRC Evaporator	$\dot{C}_5 + \dot{C}_{12} + \dot{Z}_{\text{SRCeva}} = \dot{C}_6 + \dot{C}_9$	$c_5 = c_6$
SRC Turbine	$\dot{C}_{10} + \dot{Z}_{\text{SRCtur}} = \dot{C}_9 + c_{\text{el,SRCtur}}\dot{W}_{\text{SRCtur}}$	$c_9 = c_{10}$
TEG	$\dot{C}_{10} + \dot{C}_{13} + \dot{Z}_{\text{TEG}} = \dot{C}_{11} + \dot{C}_{14}$	$c_{10} = c_{11}$, $c_{13} = 0$
SRC Pump	$\dot{C}_{11} + c_{\text{el,SRCP}}\dot{W}_{\text{SRCP}} + \dot{Z}_{\text{SRCP}} = \dot{C}_{12}$	$c_{\text{el,SRCP}} = c_{\text{el,SRCtur}}$
ORC Evaporator	$\dot{C}_6 + \dot{C}_{17} + \dot{Z}_{\text{ORCeva}} = \dot{C}_7 + \dot{C}_{18}$	$c_6 = c_7$
ORC Turbine	$\dot{C}_{18} + \dot{Z}_{\text{ORCtur}} = \dot{C}_{19} + \dot{C}_{20} + c_{\text{el,ORCtur}} \times \dot{W}_{\text{ORCtur}}$	$c_{18} = c_{19}$, $c_{18} = c_{20}$
Preheater	$\dot{C}_{21} + \dot{C}_{16} + \dot{Z}_{\text{ORCpreh}} = \dot{C}_{17} + \dot{C}_{22}$	$c_{16} = c_{17}$
Pump	$\dot{C}_{15} + c_{\text{el,ORCP}}\dot{W}_{\text{ORCP}} + \dot{Z}_{\text{ORCP}} = \dot{C}_{16}$	$c_{\text{el,ORCP}} = c_{\text{el,ORCtur}}$
Condenser	$\dot{C}_{22} + \dot{C}_{28} + \dot{Z}_{\text{ORCcon}} = \dot{C}_{23} + \dot{C}_{29}$	$c_{22} = c_{23}$, $c_{28} = 0$
Expansion Valve	$\dot{C}_{24} + \dot{Z}_{\text{EXV}} = \dot{C}_{25}$	–
Evaporator	$\dot{C}_{25} + \dot{C}_{30} + \dot{Z}_{\text{eva}} = \dot{C}_{26} + \dot{C}_{31}$	$c_{25} = c_{26}$, $c_{30} = 0$
Ejector	$\dot{C}_{32} + \dot{C}_7 + \dot{Z}_{\text{EJE}} = \dot{C}_{27}$	–
DWH	$\dot{C}_{32} + \dot{C}_7 + \dot{Z}_{\text{DWH}} = \dot{C}_{33} + \dot{C}_8$	$c_7 = c_8$, $c_{32} = 0$
PEM Electrolyzer	$c_{\text{el,PEM}}\dot{W}_{\text{PEM}} + \dot{Z}_{\text{PEM}} = \dot{C}_{34} + \dot{C}_{35}$	$c_{\text{el,PEM}} = c_{\text{el,ORCtur}}$, $c_{35} = 0$
RO desalination unit	$c_{\text{el,RO}}\dot{W}_{\text{RO}} + \dot{Z}_{\text{RO}} = \dot{C}_{37}$	$c_{\text{el,RO}} = c_{\text{el,GT}}$, $c_{36} = c_{38} = 0$

Table 5. Solar tower system validation with source results [33]

Parameter	Current study	Ref. [33]	Error [%]
$T_{\text{air},o,\text{rec}}$ [K]	1101	1101	0
$\dot{Q}_{\text{use,rec}}$ [kW]	49922	49756	0.334
η_{ex} [%]	26.77	26.73	0.18
$\dot{\text{Ex}}_D$ [kW]	87074	86659	0.48

Table 6. Validation of the Brayton gas cycle against reference results [34]

Point	Current study		Ref. [34]		Error [%]	
	P [bar]	T[K]	P [bar]	T[K]	P	T
1	1.013	298.15	1.013	298.15	0	0
2	8.634	595.51	8.6344	595.51	0.005	0
3	8.202	914.28	8.2028	914.28	0.01	0
4	7.792	1492.63	7.792	1492.63	0	0
5	1.099	987.9	1.099	987.988	0	0.009
6	1.066	718.76	1.066	718.846	0	0.012

Table 7. Validation of the ejector refrigeration cycle against reference results [35]

Variable	Current study	Ref. [35]	Error [%]
Pump power (kW)	0.02	0.0206	3.23
Vapor generator duty (kW)	9	9.115	1.28
Mass entrainment ratio	0.24	0.2436	1.52
Cooling capacity	1.75	1.7645	0.83
COP	0.19	0.1946	2.46

5 Results and Discussion

Systematic summary of the multi-output energy system under consideration is put forward in Table 8. The configuration combines gas turbines, wind turbines, ORC power plant, SRC and TEGs, to provide power, hydrogen, desalinated water, heating and cooling. The thermal efficiency (25.22%) and exergy efficiency (50.7%) of the system show the effectiveness of the system. Power outputs of the systems are given as gas turbine (20143 kW), turbine compressor (10778 kW), SRC turbine (2416 kW), ORC turbine (1286 kW), TEG (357.7 kW), and wind turbine (197 kW). The rate of destruction of the exergy is 92, 604kW, the production of hydrogen is 0.008kg/s and the production of desalinated water is19.37 kg/s. Its heating and cooling capacities are 24,050 kW and 2,904 kW respectively. Thermoelectric generator (TEG) helps to optimize the efficiency of the complete system as it transforms the waste heat into electricity. Even though it constitutes a small proportion of total production that is 1.47%, it increases power generation in the ORC by 27.81% indicating that recovery of waste heat is a factor to consider in increasing power output.

Table 8. Performance indicators and major outcomes of the proposed energy system

Parameter	Unit	Value
η_{th}	%	25.22
η_{ex}	%	50.7
$\dot{W}_{\text{GT}}$	kW	20143
$\dot{W}_{\text{comp}}$	kW	10778
$\dot{W}_{\text{SRCtur}}$	kW	2416
$\dot{W}_{\text{ORCtur}}$	kW	1286
$\dot{W}_{\text{TEG}}$	kW	357.7
$\dot{W}_{\text{wt}}$	kW	197.5
$\dot{W}_{\text{tot}}$	kW	24399
$\dot{\text{E}}\text{x}_{D,\text{tot}}$	kW	92604
$\dot{m}_{\text{H}_2}$	kg/s	0.008
$\dot{m}_{\text{FW}}$	kg/s	19.37
$\dot{Q}_{\text{heating}}$	kW	24050
$\dot{Q}_{\text{cooling}}$	kW	2904

Table 9 shows the overall results of energy and exergy analysis of the analyzed system. The compressor, with the destroyed exergy rate of 29,168 kJ/s and efficiency of 6.8%, exposes high exergy loss during the process of compression, with most of this loss being attributed to the inherent inefficiency of the unit itself-energy entering into compressor is transformed into a waste heat. Solar collector has the highest exergy efficiency of all components (97.83%) but contributes to most exergy destruction in the entire entity (51.38%). These finding highlights that the device has high capability of turning solar radiation into usable exergy. Gas turbine with an output power of 20,143 kW is the main generator of electricity as it indicates its role leading in conversion of stored chemical energy of the natural gas into work.

Table 9. Energy and exergy analysis results for system components

Components	$\dot{\text{E}}\text{x}_D$ (kW)	y_D (%)	ϵ (%)	$\dot{Q}$ or $\dot{W}$ (kW)
Compressor	29168	31.5	93.84	10778
Gas turbine	849.7	0.917	95.95	20143
Combustion chamber	9416	10.17	62.54	3390
Solar collector	47577	51.38	97.83	24050
DWH	244.4	0.264	42.85	2226
SRC Evaporator	1346	1.453	70.66	8098
SRC Turbine	575	0.621	80.77	2416
TEG	37.55	0.04	56.87	357.7
SRC Pump	2.48	0.002	90.35	25.7
PEM	717.5	0.774	49.15	1425
RO	34.19	0.036	36.49	1323
ORC Vapor Generator	787.1	0.85	1.62	4989
ORC Turbine	243.2	0.262	84.09	1286
ORC Pump	103.8	0.112	79.94	57.67
ORC Preheater	224.8	0.242	86.32	11592
ORC Condenser	589.8	0.639	0.614	13386
Ejector	220.4	0.238	21.89	-
ORC Evaporator	286	0.309	11.96	2904
Expansion Valve	45.85	0.049	90.91	-
Wind Turbine	135.6	0.146	54	197.5

Exergoeconomic data of investigated system are given in Table 10. The compressor has the cost factor (c_f) of 49.05 dollars per GJ, which is extremely inefficient as opposed to the cost factor (c_f) of solar collector and wind turbine that have much lower c_f values and hence demonstrated efficiency. The RO unit has the most exergy cost (c_p) of 82.06 dollars per GJ implying that the increase in the performance of the system by the RO unit does not correlate with the cost. The gas turbine requires the highest investment (24,876.24 dollars). The exergy-economic factor (f) measures the ratio of heat loss with the total amount that is spent on the capital. In this case it is gas turbine that performs the worst (f = 97.82%), most likely due to the

capital investment and exergy loss, whereas solar collector shows the perfect performance ($f = 100\%$). On the other hand, the local water heater gives a very low exergy-economic factor ($f = 0.16\%$) and therefore a high cost-effectiveness. Combined ability to achieve a certain level of economic efficiency is evident through the findings, which suggest that these efforts are urgently required to reduce exergy destruction inside the gas turbine and other elements.

Table 10. Results of exergoeconomic analysis for system components

Components	c_f (\$/GJ)	c_p (\$/GJ)	$\dot{C}_D \left(\frac{\$}{\text{year}} \times 10^6\right)$	$\dot{Z} \left(\frac{\$}{\text{year}}\right)$	$\dot{C}_D + \dot{Z} \left(\frac{\$}{\text{year}} \times 10^6\right)$	f (%)
Compressor	49.05	10.96	1.25	116050	1.36	7.503
Gas turbine	16.7	49.05	0.124	637393	0.762	97.82
Combustion chamber	48.21	27.89	24876	136750	24.870	0.0048
Solar collector	0	0	0	1095	0.001	100
DWH	16.7	38.97	0.036	0.6568	0.036	0.016
SRC Evaporator	16.7	11.04	1.474	632.5	1.474	2.738
SRC Turbine	11.27	35.49	0.343	119457	0.343	94.85
TEG	11.27	19.8	0.02	39163	0.020	98.93
SRC Pump	35.4	44.46	0.013	120.4	0.013	57.78
PEM	32.42	51.34	3.779	28.9	3.779	0.124
RO	49.05	82.06	8.391	47984	8.391	96.62
ORC Vapor Generator	16.7	28.92	1.318	657.4	1.318	4.76
ORC Turbine	21.42	32.42	1.341	74428	1.341	93.46
ORC Pump	32.42	44.97	2.398	203.6	2.398	5.7
ORC Preheater	13.34	18.54	0.796	7467	0.796	71.35
ORC Condenser	3.99	17.71	1.245	2277	1.245	49.16
Ejector	7.44	16.06	1.708	6.179	1.708	0.375
ORC Evaporator	19.67	60.7	0.369	2698	0.369	32.41
Expansion Valve	17.71	19.67	0.558	84	0.558	9.373
Wind Turbine	25.2	50.4	0.029	72076	0.029	53.24

The Figure 2 presents the data concerning the weighted exergy destruction rates of 20 major sources of a multi-output energy system; these are listed in decreasing order. The solar collector comes up as the most thermally unstable component whose exergy destruction rate stands at 47,577 kW because of the high-temperature gradients as well as the dramatic changes in incident solar radiation. The compressor is second with 29,168 kW, exergy destruction is high in the compressor; this is due to the fact that the compressor is characterized by inherent inefficiencies in the mechanical compression. A total of 9416 kW of exergy is destroyed with the combustion chamber itself being the cause of this exergy destruction, due to reaction irreversibilities, thermal losses, and exit of high temperature gas. Instead, exergy losses in the Organic Rankine Cycle (ORC) pump, the desalination unit, and thermoelectric (TE) generator, are low by comparison, with only under 150 kW registered by each. These results imply an unbalanced distribution of the exergy losses and show that a comparatively small group of components, namely solar collector, the compressor, and the combustion chamber, contributes most of the irreversibility of the system, thus making optimization of these entities of high priority.

In Figure 3, effective exergy of a system under compressor pressure ratio (r_p) is being represented at four turbines isentropic efficiencies (0.8, 0.85, 0.9, and 0.95). The findings reveal that increasing r_p increases exergy efficiency of all performance levels of the turbine mostly due to enhanced Brayton-cycle thermodynamics. With r_p increase expansion-work production becomes more significant, reduces irreversibilities associated with entropy production, and allows more energy to be converted more efficiently. As an example, when the turbine efficiency is 0.9, exergy efficiency increases by 21% at exergy efficiency of 44.22% ($r_p = 8$) to exergy efficiency of 53.75 ($r_p = 15$). Higher efficiencies of turbines are continuously associated with better exergy performance as it is important to focus on the turbine-design and optimum compressor operation. These results indicate the importance of accurate selection of the turbine efficiency and pressure-ratio to ensure maximum second-law efficiency depending on the multi output renewable systems.

Figure 4 indicates the effect of increasing inlet temperature in gas turbines (GT-TIT) in stages on system performance. As GT-TIT increases in temperature, say 1300 K to 2300 K, gas-turbine power increases by a factor of 2.88 or 7,862 kW to 22,892 kW

and net system power by a factor of 1.67 or 22,846 kW to 38,367 kW. At the same time, the thermal efficiency increases to 58.48% whereas the exergy efficiency advances to 50.71%. Incremental turbine growth activities are driven by an improved GT-TIT thus increasing the rate of energy conversion and reducing the thermal losses. The increased exhaust-gas temperature formed by the extraction of waste heat in lower Rankine cycles also enhances the work of lower Rankine processes, and in so doing, it raises first- and second-law efficiencies and raises the overall exergy use of the cycle. To conclude, raising the level of GT-TIT may increase power generation levels but also thermodynamic efficiency.

The effects of inlet turbine temperature on concurrent production of hydrogen and desalinated water have been outlined in Figure 5. When turbine inlet temperatures are increased to 2300 K compared to the original turbine inlet temperature of 1300 K the production of hydrogen increases to 0.0888 kg/s as opposed to 0.0797 kg/s whereas desalinated water production is increased to 24.52 kg/s as opposed to 18.7 kg/s. This will result in the increase in power production and superior coupling of thermal recovery cycles (SRC and ORC-ERC) that are at the core of both heat-based and power-driven desalination process, like reverse osmosis desalination. Increased inlet temperatures also increase the flexibility of the system since the system can produce hydrogen and water in addition to electricity with minimal effect on electricity production.

Solar thermal energy storage systems being developed are generally mounted in a manner that they absorb solar radiation which is converted into thermal energy by being heated in a receiver mode. The relationship between output temperature (T_3) and the thermal energy applied to the storage tank with the solar irradiance within 200 to 1000 $\mathrm{W/m^2}$ is shown in Figure 6. Both the temperature of the recipient and energy capacity increases with increased radiation. The output at 200 $\mathrm{W/m^2}$ is 468.67 K and the input of useful heat energy is 17 kW. With the irradiation of 1000 $\mathrm{W/m^2}$, the temperature rises to 844.67 K and the amount of thermal energy which can be stored rises to 85 kW. Wider thermal gradients and enhanced radiative heat transfer at higher temperatures are the sources of the nonlinear increase of the temperature. On the other hand, the thermal energy that was provided to the storage tank increases proportionally to DNI, confirming the scalability of the system and its effectiveness under the conditions of greater solar availability.

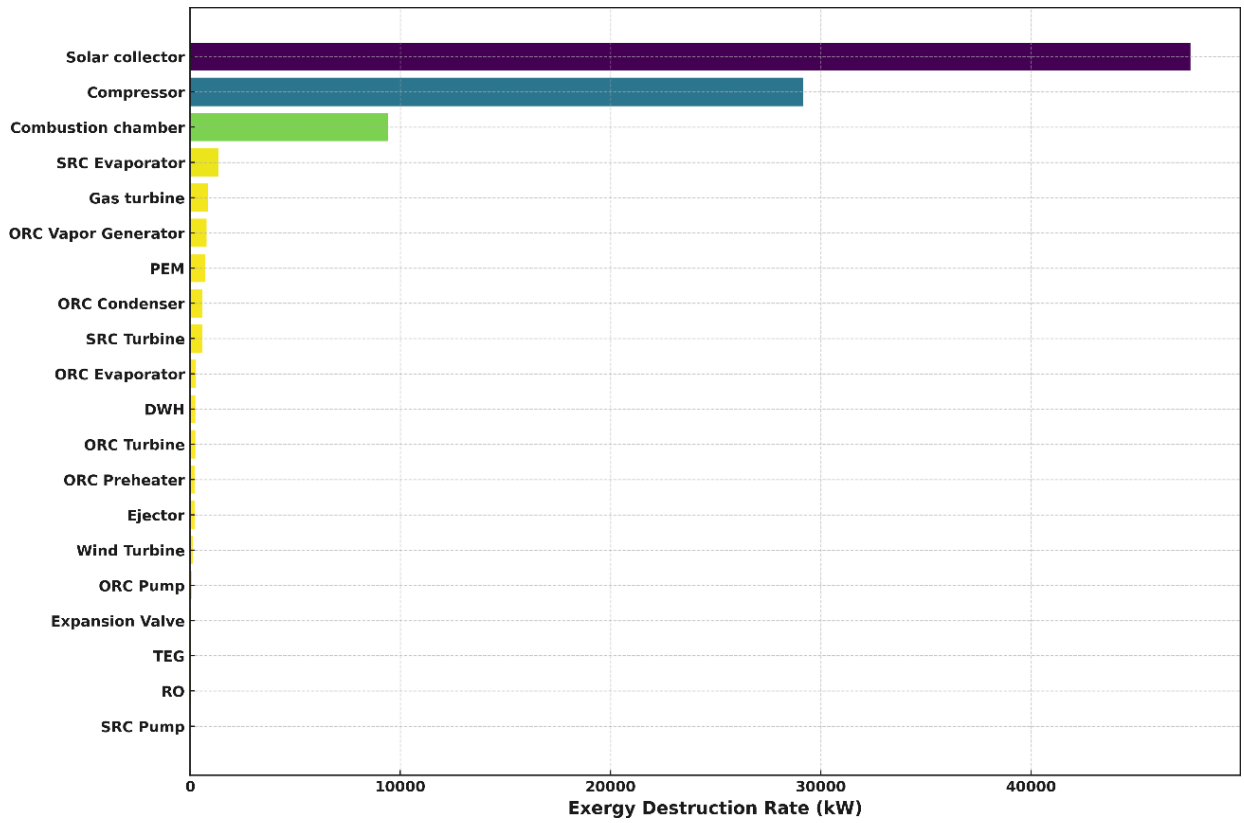

Fig. 2. Exergy destruction value for all system components.

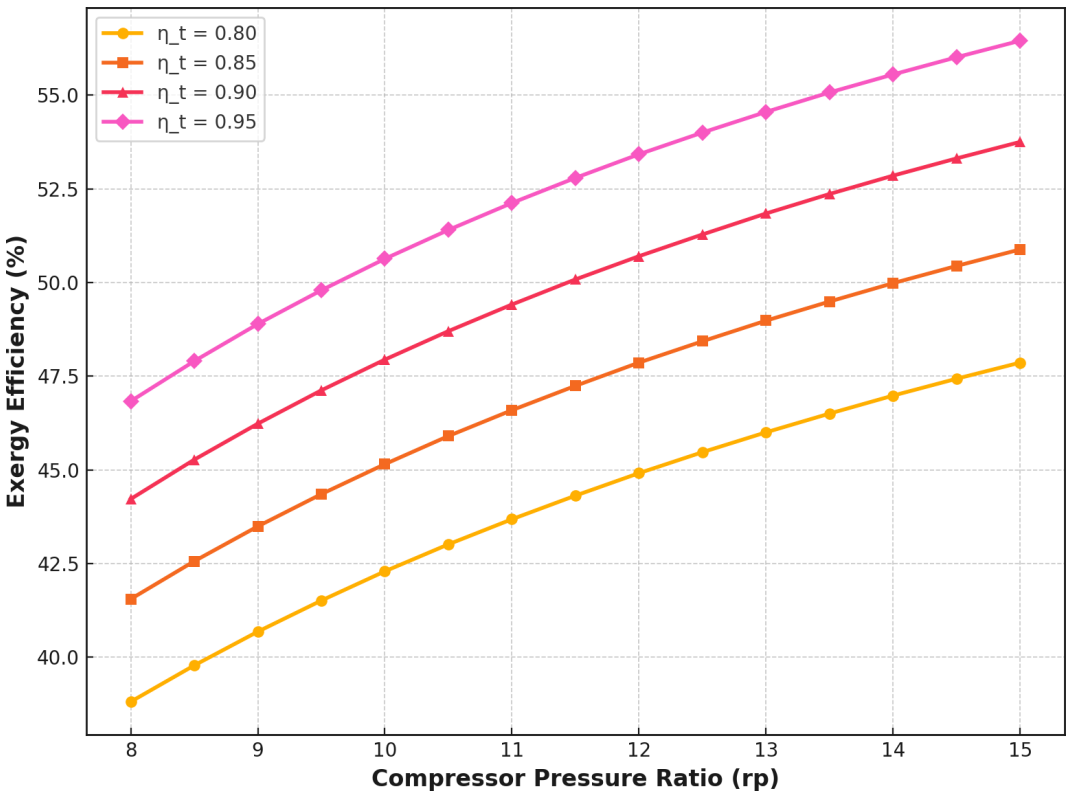

Fig. 3. Effect of compressor pressure ratio on the total system exergy efficiency at different levels of turbine isentropic efficiency.

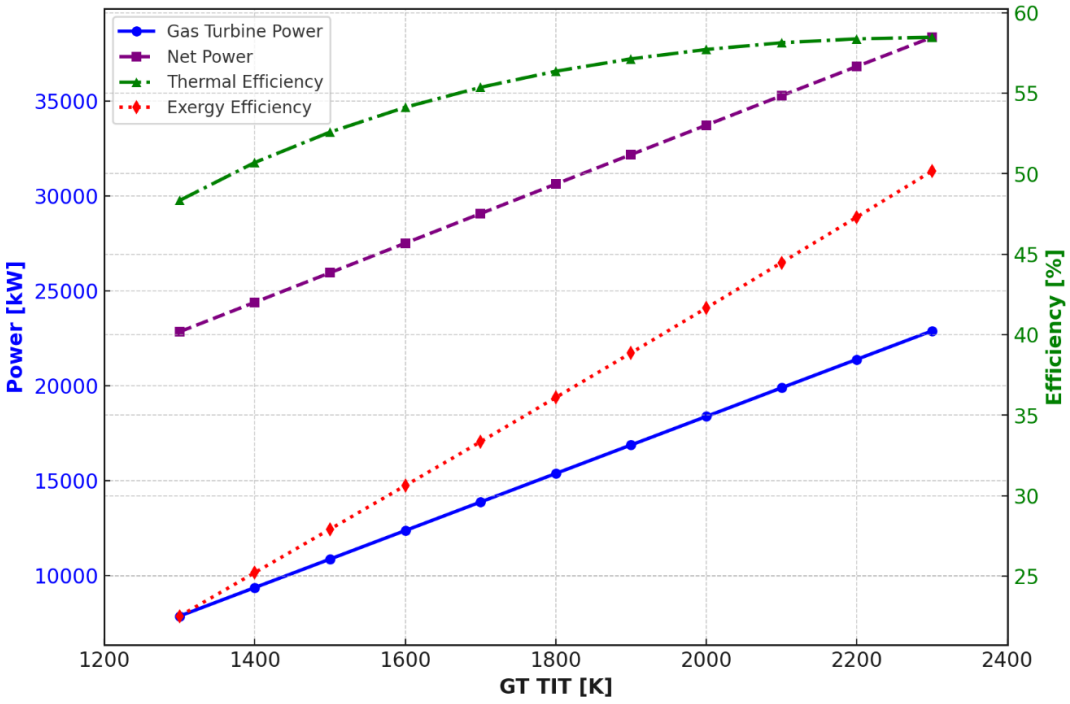

Fig. 4. The effect of gas turbine inlet temperature on the power output and thermal and exergy efficiencies of the system.

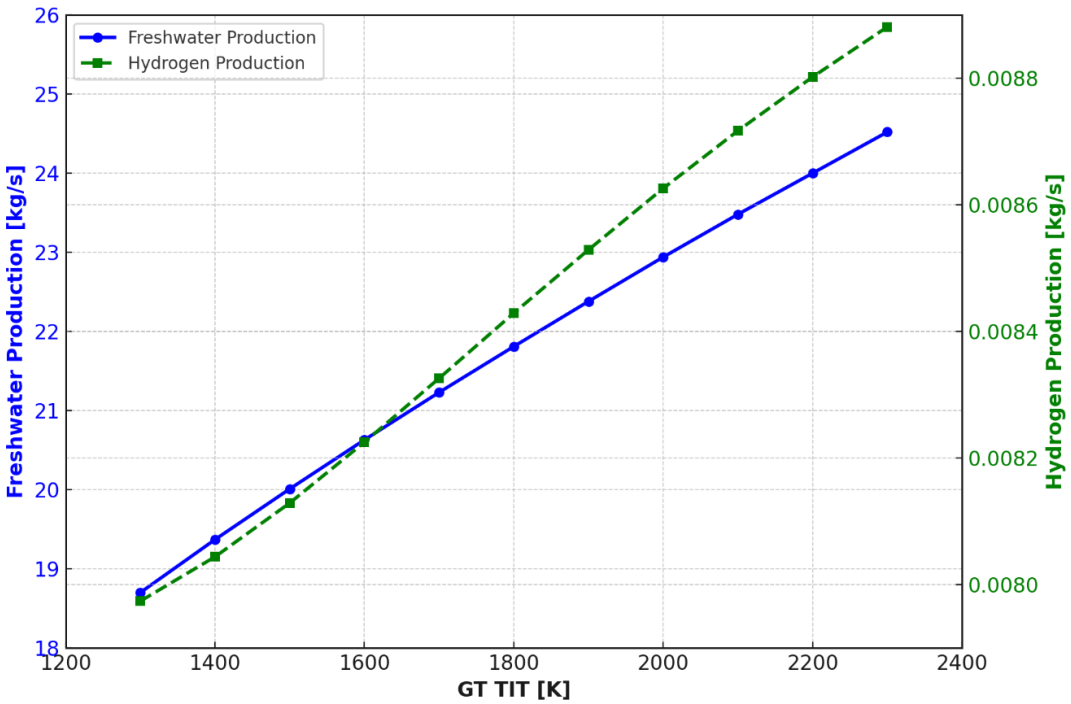

Fig. 5. Effect of gas turbine inlet temperature on the hydrogen and fresh water production rate in the system.

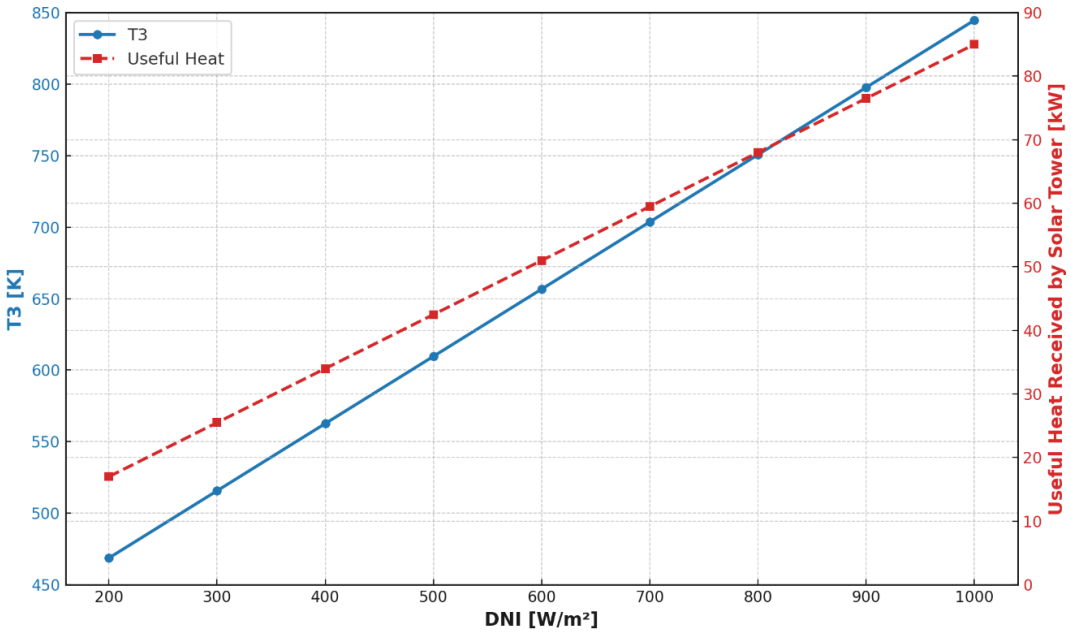

Fig. 6. Changes in collector outlet temperature and the amount of useful energy absorbed by the collector depending on the intensity of solar radiation.

Figure 7 shows the trend of the Direct Normal Irradiance (DNI) impact on net output power, thermal efficiency and the exergy efficiency in a multi-output cycle setup. When DNI increases by two times, i.e., 200 W/m^2 1000 W/m^2 to, net power increases by a factor of 1.24 or 25,177 kW to 31,407 kW and both thermal and exergy efficiencies increase by this ratio three to 26.56% to 37.48% and 51.7% to 56.78%, respectively. These improvements are significant but still, these irreversibilities within the individual subsystems e.g., the Organic Rankine Cycle (ORC) and Steam Rankine Cycle (SRC) do not permit full utilization of exergy.

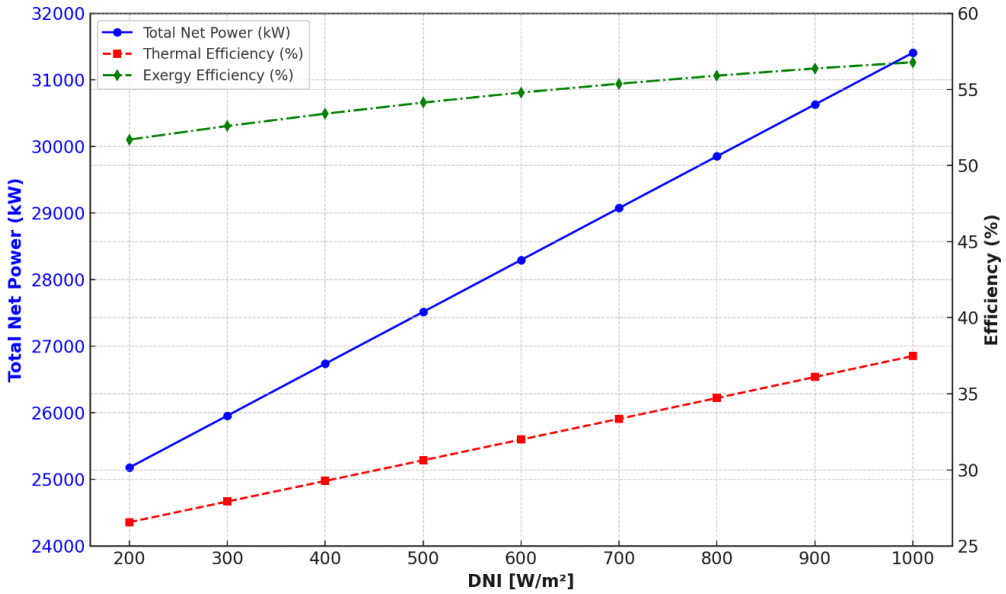

Fig. 7. Effect of solar radiation intensity on net output power, thermal efficiency and exergy efficiency.

Figure 8 explains how the wind speed affects the overall output of the net system and how wind turbines contribute to it. When the velocity of wind increases by 4 m/s to 10 m/s, the power of the turbine increases significantly in a cubic relationship, attaining the power of 1187 kW at the velocity of 10 m/s. Concurrently, net system output increases to 25,586 kW (on a comparison with 24,475 kW). Even though the input of the wind turbine is relatively small, it offers renewable energy source, and is clean, especially when there is more wind, abating the dependence on back-up combustion and increasing the system stability. This fact shows the benefit of using wind energy in conjunction with the solar-based multi-output system.

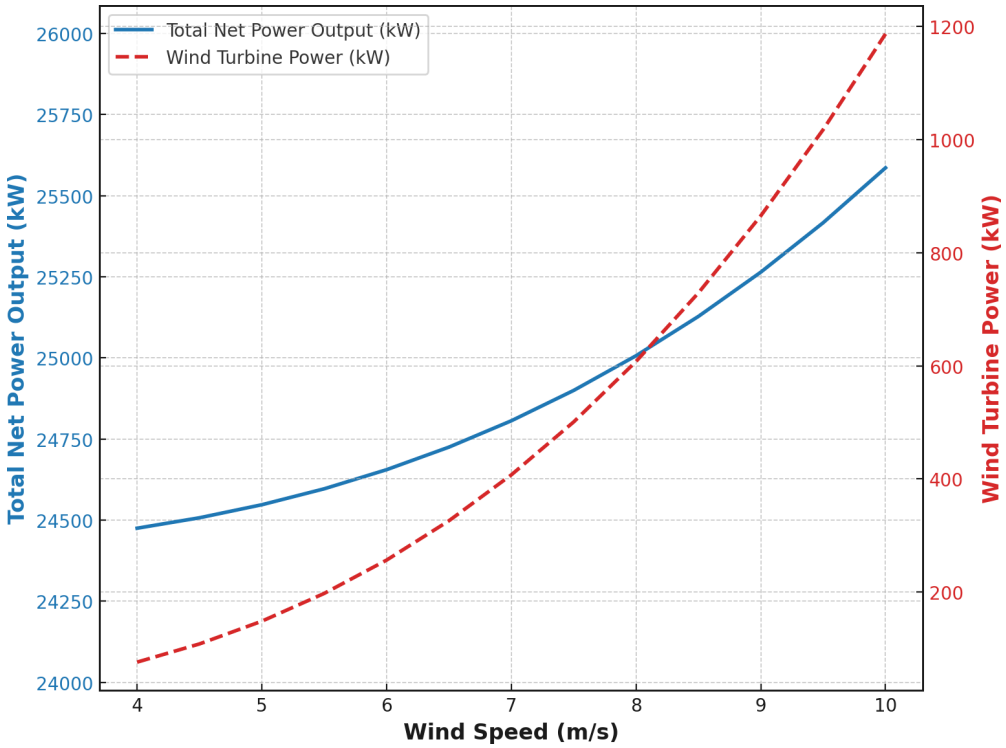

Fig. 8. The effect of wind speed on the net power of the entire system and the generated power of the wind turbine.

Figure 9 demonstrates how an increasing mass flow rate of steam Rankine cycle influences the performance of a system. As the mass flow rate of steam increases (by a factor of two) 1.5-4 kg/s the improvements in the thermal and exergy efficiency is considerable, the exergy destruction is reduced and the total output power is proportionally increased. Such results are due to increased heat recovery of gas-turbine exhaust, thus, encouraging more effective use of energy and less irreversibilities. Exergy and thermal efficiencies would increase to 55.88% and 26.5%, respectively. As a result of the change, the total generation output power increases to 26,746 kW out of 23,542 kW, which will enable a production of electricity with greater efficiency and thermal load control.

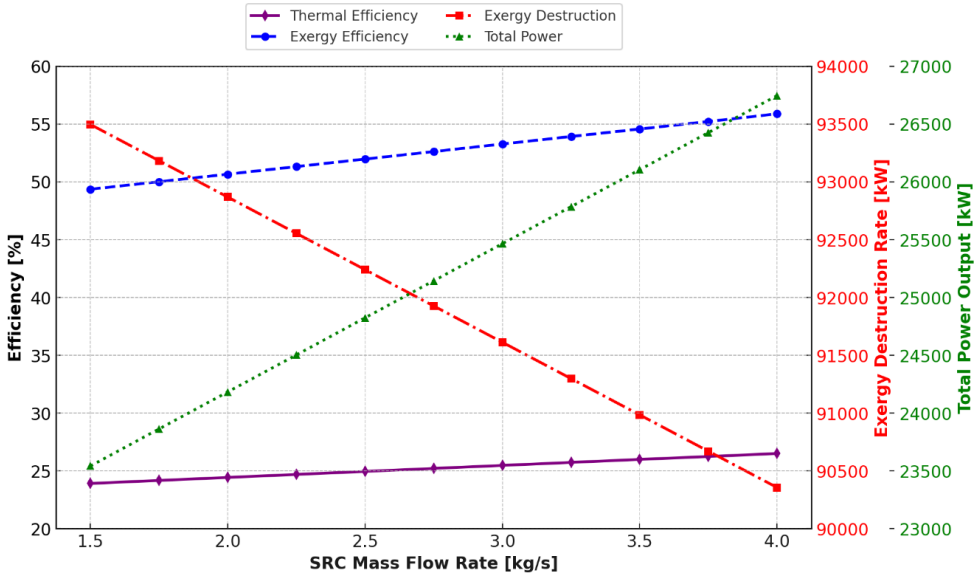

Fig. 9. Effect of increasing the mass flow rate of the steam Rankine cycle on the thermal efficiency, exergy efficiency, exergy destruction rate, and total system power.

In this section the effect of the working fluids is examined on Organic Rankine Cycle (ORC) with an ejector. The organic stipulated compounds isobutane, R134a, propane, dimethyl ether (DME) and R152a are chosen because of their good thermodynamic behavior, low impact on the environment, and zero Ozone Depletion Potential (ODP) making them viable in the renewable energy systems which are environmental-friendly. The output power of the ORC and its cooling capacity of these fluids are compared in Figure 10. DME has the greatest power and cooling capacity whereas isobutane the least. DME is suggested in cases where performance maximization and sustainability are regarded as the main goals along with its high level of energy production and low environmental impact.

In this study, we just considered some few parameters that included turbine inlet temperature and the compressor pressure ratio. We must recognize though, other elements such as the solar radiation, wind speed and the efficiency of each of the components also influence greatly on the performance of the system. To get a more clear idea of the system in different conditions a general sensitivity analysis of those would be helpful. This, we believe, would be a critical contribution to future research as a step toward the study being more realistic in terms of design and operation.

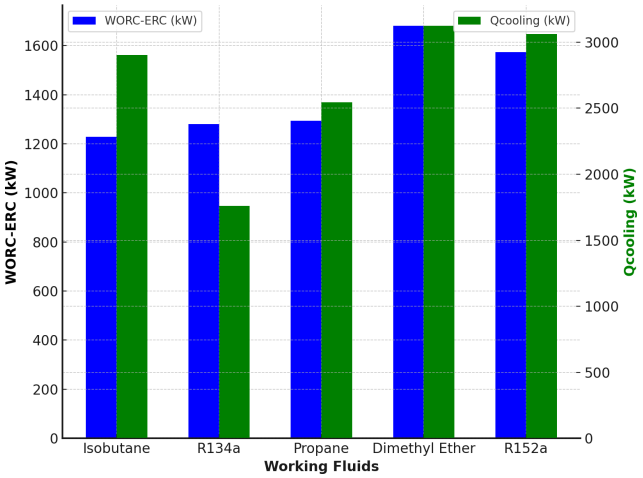

Fig. 10. Comparison of output power and cooling power for different working fluids in an organic Rankine system with an ejector.

6 Conclusions

In this study, a solar-wind multigeneration system has been presented that can generate electricity and hydrogen, fresh water, heating and cooling of the same platform. The system could obtain 38.37 MW of electricity, 0.008 kg/s of hydrogen, 19.37 kg/s of desalinated water, 24.05 MW of thermal energy, and 2.90 MW of cooling. The total performance of 25.22% (thermal efficiency) and 50.7% (exergy efficiency) could be achieved thanks to the synergy of three recovery cycles (ORC, SRC and TEG). The analysis showed that the largest portion of exergy losses had been in the solar collector, compressor, and combustion chamber, and identifying the component in which to make improvements would have a significant positive effect. The economical analysis revealed that, although the gas turbine is the most capital-intensive component, the solar and wind subsystems produce high cost-effectiveness, and performance could be improved further by tailoring the turbine speed parameter, the inlet temperature and compressor pressure ratio. Practically, this kind of system is the most promising where there is the high sun radiation and constant wind.

The upfront costs are high, although decreasing renewable technology costs, in conjunction with policy incentives (hydrogen subsidies and carbon credits), may make real-world application more enticing. The proposed implementation of multigeneration is superior to conventional trigeneration systems, and, besides the electricity, heating, and cooling, it gives two more resources: freshwater and hydrogen production. This not only limits redundancy in energy services but also increases resilience of regions that are prone to water shortages or those who are in need of clean energy fuels. All these findings indicate combined that solar energy coming together with wind energy multigeneration is not only technically possible and cost effective, but also a viable step towards development of cleaner multi-purpose energy systems.

Nomenclature

Symbol / Acronym	Definition	Unit
T	Temperature	K
P	Pressure	kPa
W	Work / Power	kW
m	Mass flow rate	kg/s
η	Efficiency	–
ρ	Density	kg/m^3
DNI	Direct Normal Irradiance	W/m^2
LCOE	Levelized Cost of Energy	USD/kWh
ODP	Ozone Depletion Potential	–
PV	Photovoltaic	–
WT	Wind Turbine	–
ORC	Organic Rankine Cycle	–
SRC	Steam Rankine Cycle	–
ERC	Ejector Refrigeration Cycle	–
PEM	Proton Exchange Membrane (electrolyzer)	–
RO	Reverse Osmosis (desalination)	–
TES	Thermal Energy Storage	–
TEG	Thermoelectric Generator	–
TIT	Turbine Inlet Temperature	K
GT	Gas Turbine	–
HS	Heat Sink / Heat Source	–
EES	Engineering Equation Solver (software)	–
USD	United States Dollar	–

References

[1] Chong W, Naghavi M, Poh S, Mahlia T, Pan K. Techno-economic analysis of a wind–solar hybrid renewable energy system with rainwater collection feature for urban high-rise application. Applied Energy. 2011;88(11):4067-77.

[2] Gao J, Zhang Y, Li X, Zhou X, Kilburn ZJ. Thermodynamic and thermoeconomic analysis and optimization of a renewable-based hybrid system for power, hydrogen, and freshwater production. Energy. 2024;295:131002.

[3] Ashfaq A, Kamali ZH, Agha MH, Arshid H. Heat coupling of the pan-European vs. regional electrical grid with excess renewable energy. Energy. 2017;122:363-77.

[4] Sharifishourabi M, Dincer I, Mohany A. Development and assessment of a new solar-geothermal based integrated energy system with sonic hydrogen generation for buildings. Journal of Building Engineering. 2023;80:107944.

[5] Forghani AH, Solghar AA, Hajabdollahi H. Optimal design of a multi-generation system based

on solar and geothermal energy integrated with multi-effect distillatory. Applied Thermal Engineering. 2024;236:121381.

[6] Azizi S, Nedaei N, Yari M. Proposal and evaluation of a solar-based polygeneration system: development, exergoeconomic analysis, and multi-objective optimization. International Journal of Energy Research. 2022;46(10):13627-56.

[7] Mahmoudan A, Samadof P, Hosseinzadeh S, Garcia DA. A multigeneration cascade system using ground-source energy with cold recovery: 3E analyses and multi-objective optimization. Energy. 2021;233:121185.

[8] Li K, Ding YZ, Ai C, Sun H, Xu YP, Nedaei N. Multi-objective optimization and multi-aspect analysis of an innovative geothermal-based multigeneration energy system for power, cooling, hydrogen, and freshwater production. Energy. 2022;245:123198.

[9] Javadi MA, Abhari MK, Ghasemiasl R, Ghomashi H. Energy, exergy and exergy-economic analysis of a new multigeneration system based on double-flash geothermal power plant and solar power tower. Sustainable Energy Technologies and Assessments. 2021;47:101536.

[10] Mahmoudan A, Esmaeilion F, Hoseinzadeh S, Soltani M, Ahmadi P, Rosen M. A geothermal and solar-based multigeneration system integrated with a TEG unit: development, 3E analyses, and multi-objective optimization. Applied Energy. 2022;308:118399.

[11] Mohammadi M, Mahmoudan A, Nojedehi P, Hoseinzadeh S, Fathali M, Garcia DA. Thermo-economic assessment and optimization of a multi-generation system powered by geothermal and solar energy. Applied Thermal Engineering. 2023;230:120656.

[12] Koc M, Yuksel YE, Ozturk M. Thermodynamic and exergo-economic assessments of a new geothermally driven multigeneration plant. International Journal of Hydrogen Energy. 2022;47(45):19463-80.

[13] Khan MS, Abid M, Bashir MA, Amber KP, Khanmohammadi S, Yan M. Thermodynamic and exergoeconomic analysis of a novel solar-assisted multigenerational system utilizing high temperature phase change material and hybrid nanofluid. Energy Conversion and Management. 2021;236:113948.

[14] Ding GC, Peng J, Mei-Yun G. Technical assessment of Multi-generation energy system driven by integrated renewable energy Sources: Energetic, exergetic and optimization approaches. Fuel. 2023;331:125689.

[15] Sen O, Guler OF, Yilmaz C, Kanoglu M. Thermodynamic modeling and analysis of a solar and geothermal assisted multi-generation energy system. Energy Conversion and Management. 2021;239:114186.

[16] Guler OF, Sen O, Yilmaz C, Kanoglu M. Performance evaluation of a geothermal and solar-based multigeneration system and comparison with alternative case studies: Energy, exergy, and exergoeconomic aspects. Renewable Energy. 2022;200:1517-32.

[17] Sezer N, Koç M. Development and performance assessment of a new integrated solar, wind, and osmotic power system for multigeneration, based on thermodynamic principles. Energy Conversion and Management. 2019;188:94-111.

[18] Ozlu S, Dincer I. Development and analysis of a solar and wind energy based multigeneration system. Solar Energy. 2015;122:1279-95.

[19] Nasrabadi AM, Korpeh M. Techno-economic analysis and optimization of a proposed solar-wind-driven multigeneration system; case study of Iran. International Journal of Hydrogen Energy. 2023;48(36):13343-61.

[20] Mahmood Mejbel Ghrairi S, Khalilian M, Mirzaee I. Thermodynamic and thermoeconomic analysis of a multigeneration system using solar and geothermal energies. Hydrogen, Fuel Cell & Energy Storage. 2025;12(1):19-30.

[21] Abdollahi SA, Faramarzi S, Mafi M, Ranjbar SF, Motavalli Sofiani S. Proposing a Hydrogen Liquefaction Cycle for Geothermal Energy Storage in an Innovative Multi-Generation System. Hydrogen, Fuel Cell & Energy Storage. 2025;12(1):1-8.

[22] Klein SA. Engineering equation solver version 9, professional version. McGraw-Hill; 2013.

[23] Zoghi M, Habibi H, Chitsaz A, Shamsaiee M. Exergoeconomic and environmental analyses of a novel trigeneration system based on combined gas turbine-air bottoming cycle with hybridization of solar power tower and natural gas combustion. Applied Thermal Engineering. 2021;188:116610.

[24] Falcão D, Pinto A. A review on PEM electrolyzer modelling: Guidelines for beginners. Journal of cleaner production. 2020;261:121184.

[25] Vince F, Marechal F, Aoustin E, Bréant P. Multi-objective optimization of RO desalination plants. Desalination. 2008;222(1-3):96-118.

[26] Azad A, Shateri H. Design and optimization of an entirely hybrid renewable energy system (WT/PV/BW/HS/TES/EVPL) to supply electrical and thermal loads with considering uncertainties in generation and consumption. Applied Energy. 2023;336:120782.

[27] Bejan A. Advanced engineering thermodynamics. John Wiley & Sons; 2016.

[28] Yilmaz F. Thermodynamic performance evaluation of a novel solar energy based multigeneration system. Applied Thermal Engineering. 2018;143:429-37.

[29] Zhang M, Chen H, Zoghi M, Habibi H. Comparison between biogas and pure methane as the fuel of a polygeneration system including a regenerative gas turbine cycle and partial cooling supercritical CO_2 Brayton cycle: 4E analysis and tri-objective optimization. Energy. 2022;257:124695.

[30] Mehrenjani JR, Gharehghani A, Nasrabadi AM, Moghimi M. Design, modeling and optimization of a renewable-based system for power generation and hydrogen production. International Journal of Hydrogen Energy. 2022;47(31):14225-42.

[31] Gao J, Zhang Y, Li X, Zhou X, Kilburn ZJ. Thermodynamic and thermoeconomic analysis and optimization of a renewable-based hybrid system for power, hydrogen, and freshwater production. Energy. 2024;295:131002.

[32] Khanmohammadi S, Atashkari K, Kouhikamali R. Exergoeconomic multi-objective optimization of an externally fired gas turbine integrated with a biomass gasifier. Applied Thermal Engineering. 2015;91:848-59.

[33] Ashikuzzaman A, Adnan S. Optical efficiency comparison of circular heliostat fields: Engender of hybrid layouts. Renewable Energy. 2021;178:506-19.

[34] Toffolo A, Lazzaretto A. Evolutionary algorithms for multi-objective energetic and economic optimization in thermal system design. Energy. 2002;27(6):549-67.

[35] Zheng B, Weng Y. A combined power and ejector refrigeration cycle for low temperature heat sources. Solar Energy. 2010;84(5):784-91.